Supporting Information

Nanostructuring-Synergetic Base-Stacking Effect: An Enhanced Versatile Sandwich Sensor Enables Ultrasensitive Detection of MicroRNAs in Blood

Xin-Xin Peng,[1] Tongtong Guo,[2] Hao Lu,[1] Linlin Yue,[1] You Li,[1,3] Dan Jin,[1] Guo-Jun Zhang,[1]* Fan Yang[2]*

[1]School of Laboratory Medicine, Hubei University of Chinese Medicine, Wuhan 430065, China
[2]School of Pharmacy, Guangxi Medical University, Nanning 530021, China
[3]Department of Medical Laboratory, the Central Hospital of Wuhan, Tongji Medical College, Huazhong University of Science and Technology, Wuhan 430014, China
*Email: zhanggj@hbtcm.edu.cn; yangfan@gxmu.edu.cn

Table of contents

Table S1. Involved oligonucleotides and corresponding sequences

Name	Sequence (5'-3')
9 nt CP$^{\delta}$	HS-$(CH_2)_6$-TCAACATCA
13 nt SP$^{\delta}$	GTCTGATAAGCTA
10 nt CP$^{\delta}$	HS-$(CH_2)_6$-TCAACATCAG
12 nt SP$^{\delta}$	TCTGATAAGCTA
11 nt CP$^{\delta}$	HS-$(CH_2)_6$-TCAACATCAGT
11 nt SP$^{\delta}$	CTGATAAGCTA
12 nt CP$^{\delta}$	HS-$(CH_2)_6$-TCAACATCAGTC
10 nt SP$^{\delta}$	TGATAAGCTA
13 nt CP$^{\delta}$	HS-$(CH_2)_6$-TCAACATCAGTCT
9 nt SP$^{\delta}$	GATAAGCTA
14 nt CP$^{\delta}$	HS-$(CH_2)_6$-TCAACATCAGTCTG
8 nt SP$^{\delta}$	ATAAGCTA
22nt CP$^{\delta}$	HS-$(CH_2)_6$-TCAACATCAGTCTGATAAGCTA
DNA21-MB$^{\delta}$	TAGCTTATCAGACTGATGTTGA-MB
miR21	UAGCUUAUCAGACUGAUGUUGA
miR21-Biotin-SP	TCTGATAAGCTA-TTTTTT-Biotin
miR223	UGUCAGUUUGUCAAAUACCCCA
miR223-CP	HS-$(CH_2)_6$-TGGGGTATTT
miR223-Biotin-SP	GACAAACTGACA-TTTTTT-Biotin
miR141	UAACACUGUCUGGUAAAGAUGG
miR141-CP	HS-$(CH_2)_6$-CCATCTTTAC
miR141-Biotin-SP	CAGACAGTGTTA-TTTTTT-Biotin
miR10b	UACCCUGUAGAACCGAAUUUGUG
miR10b-CP	HS-$(CH_2)_6$-CACAAATTCG
miR10b-Biotin-SP	GTTCTACAGGGTA-TTTTTT-Biotin

Name	Sequence (5’-3’)
SM-miR21	UAGCUUAUCAGACUGAUAUUGA
TM-miR21	UAGAUUAUCAGACUGAUAUUGA
Random-RNA	UUGUACUACACAAAAGUACUG

CP: capture probe
SP: stacking probe
MB: methylene blue
[δ] labeled sequences were used in optimal HS-DNA CP selection.
The mismatched bases were marked in red.

Table S2. T_m of different length of CPs (9 nt to 14 nt) and corresponding SPs (13 nt to 8 nt).

Name	T_m	Name	T_m	ΔT_m
9 nt CP	12.5	13 nt SP	32.0	16.5
10 nt CP	22.5	12 nt SP	27.2	4.7
11 nt CP	27.3	11 nt SP	23.2	4.1
12 nt CP	32.0	10 nt SP	17.0	15.0
13 nt CP	35.1	9 nt SP	10.8	24.3
14 nt CP	38.8	8 nt SP	0.9	37.9

Table S3. Free energy of prehybridization mixtures (SP and DNA21) and direct hybridization mixtures (CP and DNA21)

Name	Free energy (F)	Name	Free energy (F)	Δ F
13nt SP+D-21	-10.41	9 nt CP+D-21	-13.4	2.99
12nt SP +D-21	-17.12	10 nt CP +D-21	-15.7	1.42
11nt SP +D-21	-16.4	11 nt CP +D-21	-16.75	0.35
10nt SP +D-21	-14.06	12 nt CP +D-21	-18.51	4.45
9nt SP +D-21	-13.29	13 nt CP +D-21	-19.59	6.3
8nt SP +D-21	-10.8	14 nt CP +D-21	-27.78	16.98

D-21: DNA21;
The unit of free energy is kcal/mol.

Table S4. Comparison between our sensor and other similar sensors for miRNA detection.

Methods	Targets	Linear range	Sensitivity	Ref[a]
Fluorescence	miR21	0-16 nM	47 pM	1
SERS	miR21	1 pM-10 nM	1 pM	2
Colorimetric	miR21	150 fM-3 nM	70 fM	3
Photoelectrochemistry	miR21	1 pM-100 nM	31 fM	4
Electrochemical	miR21	140 pM-10 nM	40 pM	5
FRET	miR21	100 pM-200 nM	100 pM	6
Fluorescence	let-7a	100 fM-1 nM	58 fM	7
Chemiluminescence	miR122	80 pM-100 nM	49.6 fM	8
Electrochemical	miR21	10 fM-1 nM	79.3 aM	This work

SERS: surface-enhanced Raman scattering
FRET: fluorescence resonance energy transfer
[a]References at the end of SI

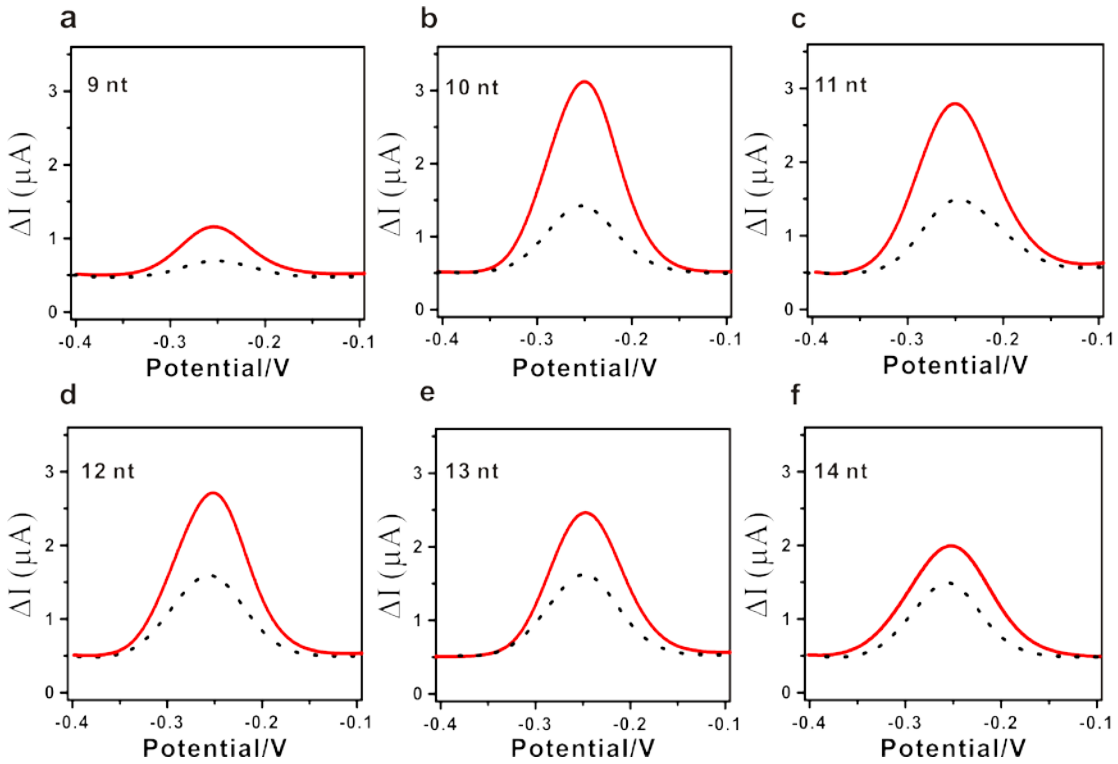

Figure S1. Square wave voltammetry (SWV) curves of the sensor assembled with 0.5 μM 9-14 nt HS-DNA CPs (a: 9 nt; b: 10 nt; c: 11 nt; d: 12 nt; e: 13 nt; f: 14 nt), in response to 1 μM DNA21-MB with (sandwich structure (I_S): red line) or without 2 μM corresponding reporter probes (direct CP-TS hybridization (I_H): dark dot) in 10 mM PBS (pH = 7.4) at room temperature.

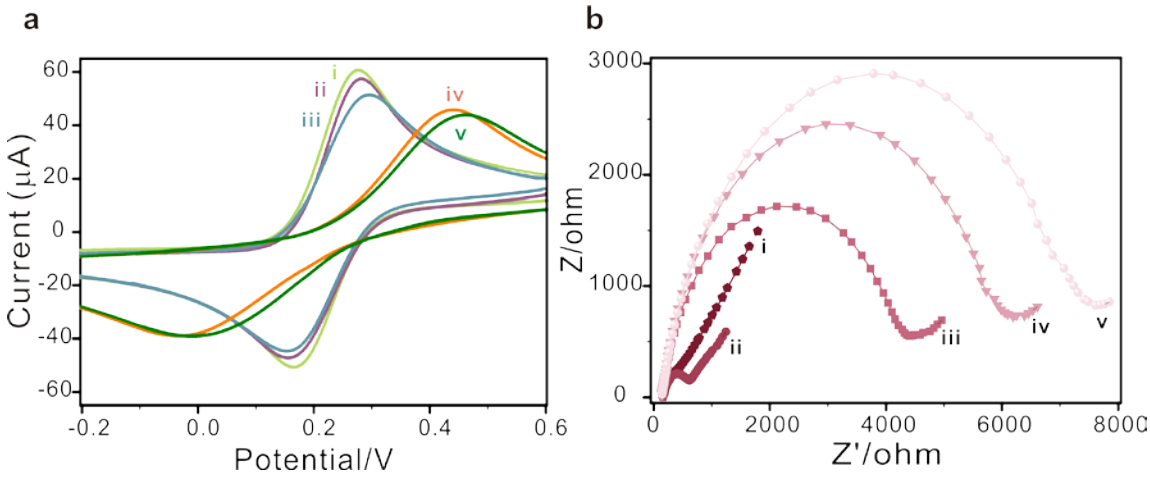

Figure S2. To verify the successful assembly of probes on the sensor, cyclic voltammetry (CV) and electrochemical impedance spectroscopy (EIS) were employed to characterize the step by step construction of the sensing interface using the redox pair of $[Fe(CN)_6]^{3-/4-}$. A typical CV response of bare gold electrode (GE) was obtained (line i in a) with minimal electro-transfer resistance (R_{et}) (curve i in b), reflecting the barrier-free diffusion of $[Fe(CN)_6]^{3-/4-}$ to the bare gold electrode. After the immobilization of HS-DNA CPs, there is an increment in peak separation of CV (line ii in a), owning to the negatively charged phosphate backbone in DNA probes. Similarly, R_{et} also increased because of the improved repulsion between charged DNA and $[Fe(CN)_6]^{3-/4-}$ (curve ii in b). After blocking by MCH, there were further changes of CV (line iii in a) and R_{et} (curve iii in b). As the prehybridized duplex was captured on the interrogating electrode, the peak current continued to reduce and an increase in peak separation emerged (line iv in a). There is also an increment for R_{et} (curve iv in b). Finally, when we apply avidin-HRP, we can also see changes of CV and EIS (line v in a, and curve v in b). Overall, these results indicated the successful preparation of our sensor. Electrochemical measurement in 0.1 M KCl solution containing 5 mM $[Fe(CN)_6]^{3-/4-}$ by scanning the potential from -0.2 to 0.6 V at a scan rate of 100 mV/s.

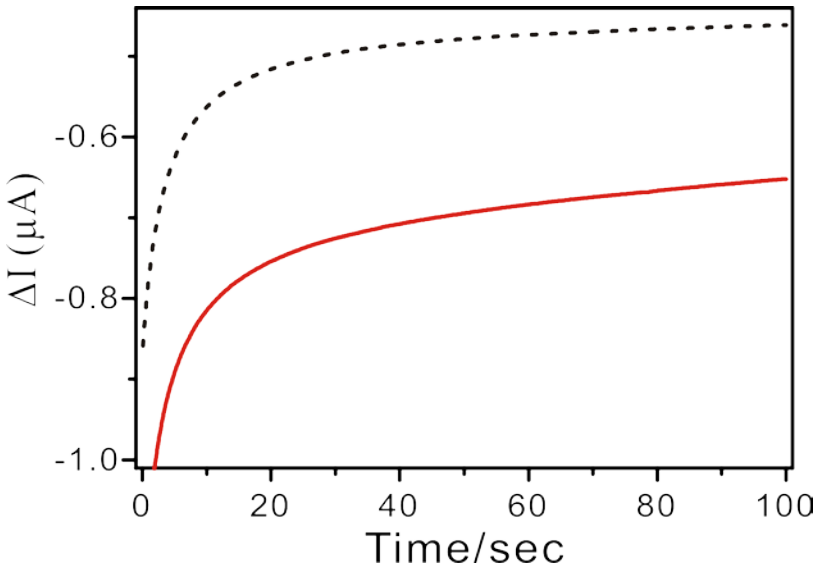

Figure S3. The feasibility of Bsee-miR sensor implemented HRP-TMB signal amplification. Amperometric i-t curve of 1 pM 10 nt HS-DNA CP incubation with miR21-Biotin-SP (2 μM)-miR21 (1 pM) prehybridization complexes and SA-HRP (red line) or miR21-Biotin-SP (2 μM)-PBS complexes and SA-HRP (dark dot) in TMB at room temperature.

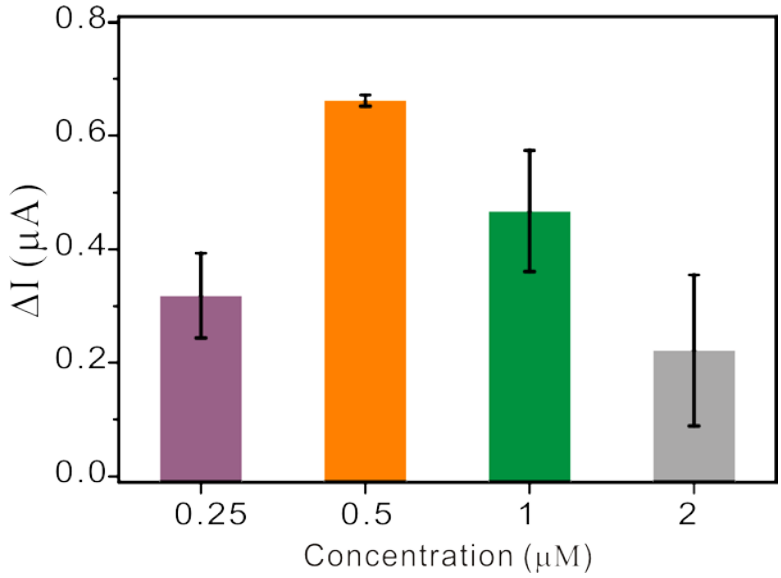

Figure S4. Assembly concentrations of HS-DNA CP ranging from 0.25 μM to 2 μM in Bsee-miR sensor were optimized (in the presence of 10 nM target miR21 and 20 nM biotin stacking probe) to obtain the maximal hybridization efficiency and the minimal steric hindrance, as well as to maintain highly ordered molecular orientation at biointerface. Error bars show the standard deviations of measurements taken from at least three independent experiments.

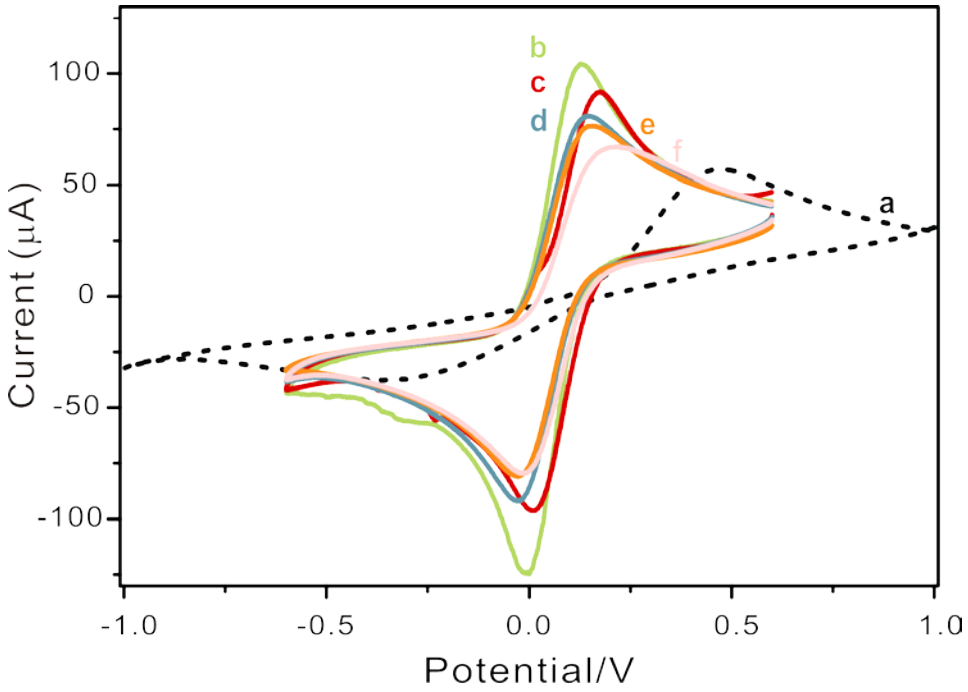

Figure S5. Cyclic voltammetry characterization of stepwise modification of nanostructuring-enhanced Bsee-miR sensor. (a) bare SPCE; (b) SPCE decorated with gold nanostructures (AuNS-SPCE); (c) HS-DNA CPs assembled on AuNS-SPCE via Au-S bond; (d) Passivation by MCH; (e) Target miR21 and biotinylated stacking probe complexes were captured on AuNS-SPCE; (f) Introduction of 1% BSA to block the nonspecific sites. The CV was carried out in 0.1 M KCl solution containing 5 mM $[Fe(CN)_6]^{3-/4-}$ at a scan rate of 100 mV/s.

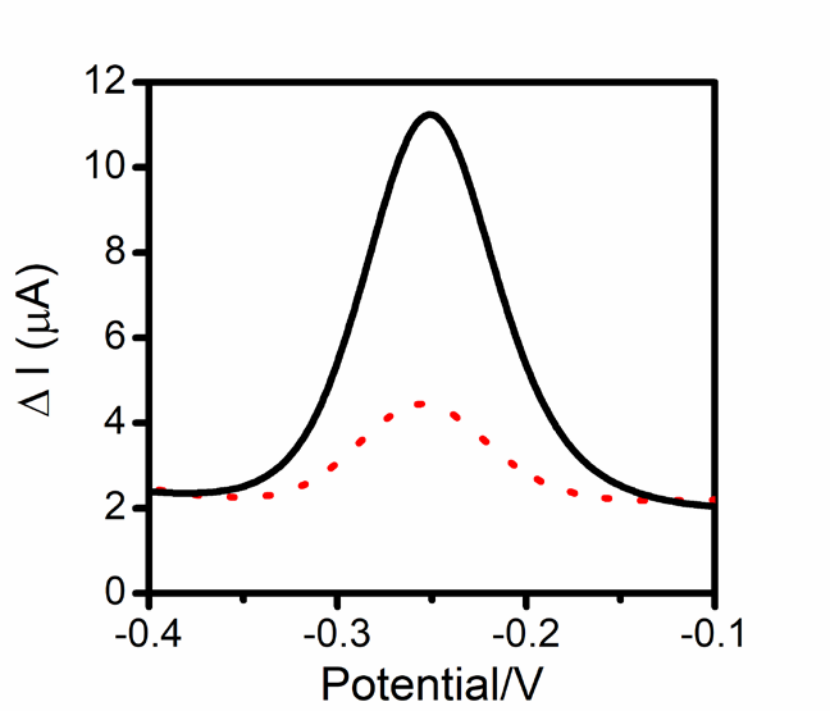

Figure S6. Square wave voltammetry (SWV) curves of AuNS-SPCE based Bsee-miR sensor incubating with 0.5 μM 10nt HS-DNAs 1 μM DNA-21-MB and 2 μM corresponding probes (experimental group: black line) or PBS (control group: red dot) in 10 mM PBS (pH = 7.4) at room temperature.

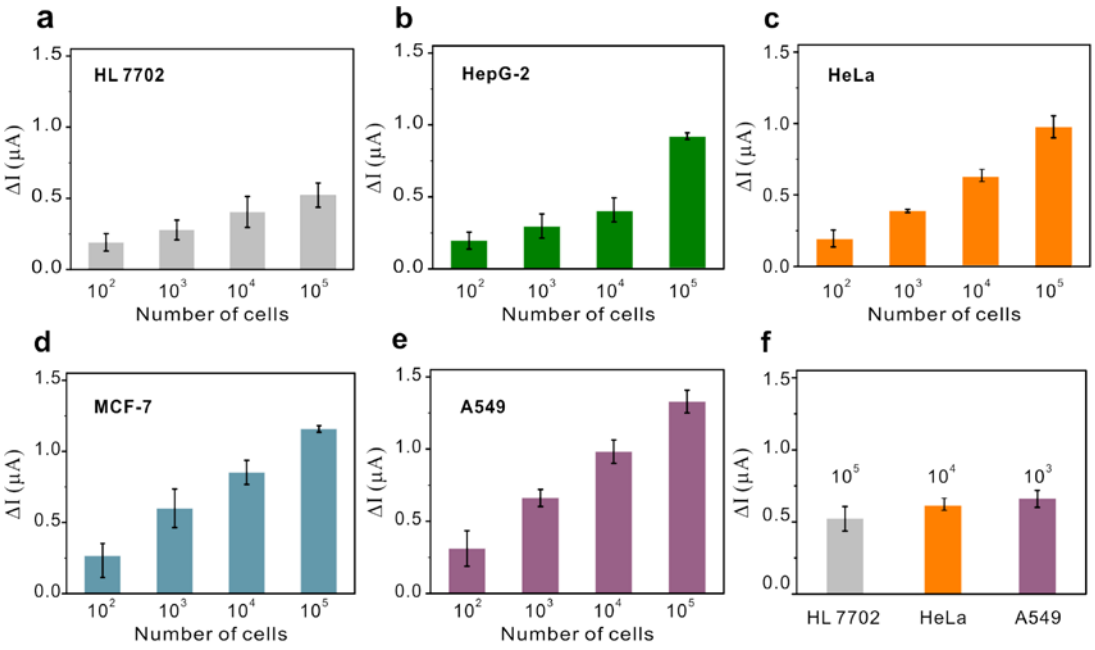

Figure S7. Nanostructuring-enhanced Bsee-miR sensor allows for detection of the target miR21 from total RNA extracted from A549 (a), MCF-7 (b), HeLa (c), HepG-2 (d) cells and HL7702 cells (e) with different numbers (10^2, 10^3, 10^4 and 10^5 cells), respectively. (f) Comparison of signal changes in response to HL7702, HepG-2 and A549 with distinct cell numbers. Error bars represent the standard deviations of measurements (n = 3).

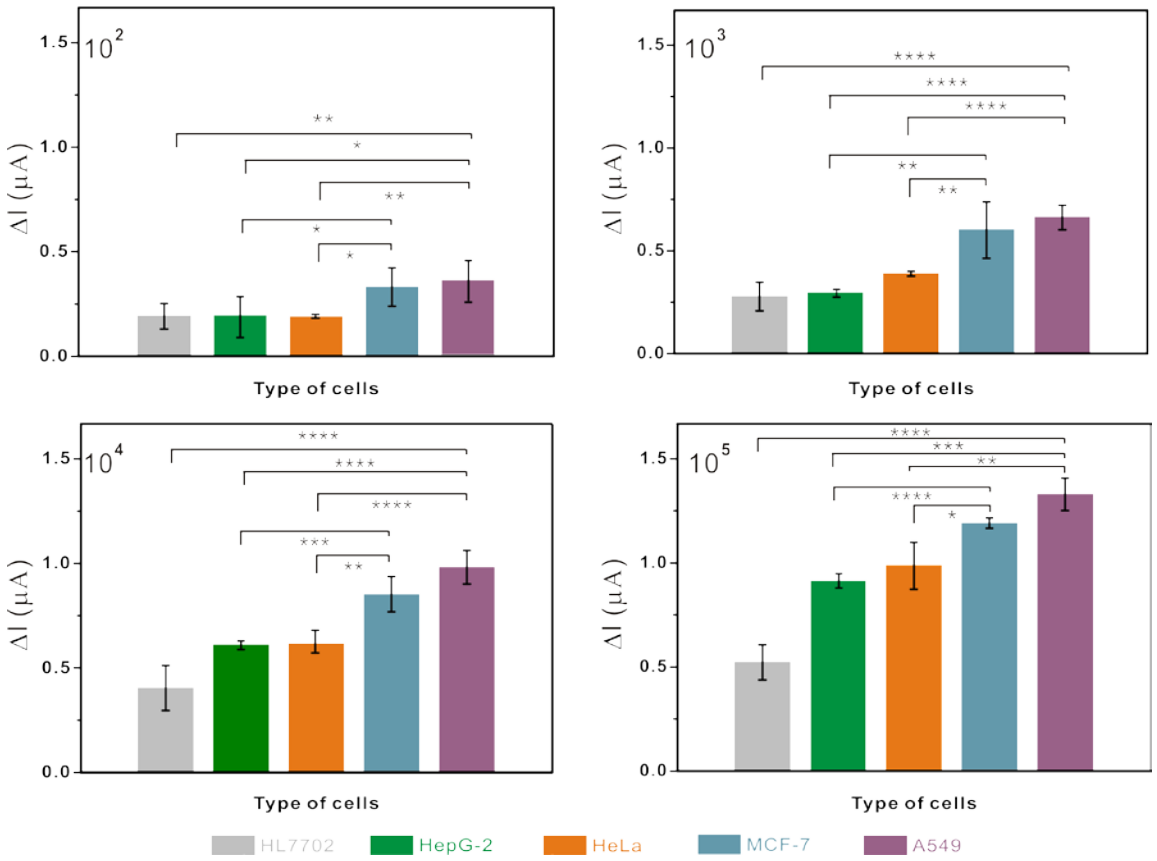

Figure S8. The difference of nanostructuring-enhanced Bsee-miR sensor in detection of total RNA from different cells. T test was used to prove the over-expression of miR21 in A549 and MCF-7 cells relative to HepG-2 and HeLa, as well as HL7702.

References

[1] Zhen, S. J.; Xiao, X.; Li, C. H.; Huang, C. Z. An Enzyme-Free DNA Circuit-Assisted Graphene Oxide Enhanced Fluorescence Anisotropy Assay for MicroRNA Detection with Improved Sensitivity and Selectivity. *Anal. Chem.* **2017,** *89* (17), 8766-8771.

[2] Su, J.; Wang, D.; Nörbel, L.; Shen, J.; Zhao, Z.; Dou, Y.; Peng, T.; Shi, J.; Mathur, S.; Fan, C.; Song, S. Multicolor Gold–Silver Nano-Mushrooms as Ready-to-Use SERS Probes for Ultrasensitive and Multiplex DNA/miRNA Detection. *Anal. Chem.* **2017,** *89* (4), 2531-2538.

[3] Guo, Q.; Bian, F.; Liu, Y.; Qu, X.; Hu, X.; Sun, Q. Hybridization chain reactions on silica coated Qbeads for the colorimetric detection of multiplex microRNAs. *Chem Comm.* **2017,** *53* (36), 4954-4957.

[4] Chu, Y.; Wu, R.; Fan, G.-C.; Deng, A.-P.; Zhu, J.-J. Enzyme-Free Photoelectrochemical Biosensor Based on the Co-Sensitization Effect Coupled with Dual Cascade Toehold-Mediated Strand Displacement Amplification for the Sensitive Detection of MicroRNA-21. *ACS Sustain.Chem. Eng.* **2018,** *6* (9), 11633-11641.

[5] Campuzano, S.; Torrente-Rodríguez, R. M.; López-Hernández, E.; Conzuelo, F.; Granados, R.; Sánchez-Puelles, J. M.; Pingarrón, J. M. Magnetobiosensors based on viral protein p19 for microRNA determination in cancer cells and tissues. *Angew. Chem. Int. Ed.* **2014,** *53*, 6168-6171.

[6] Universal Fluorescence Biosensor Platform Based on Graphene Quantum Dots and Pyrene-Functionalized Molecular Beacons for Detection of MicroRNAs. *ACS Appl. Mater. Interfaces* **2015,** *7*, 16152-16156.

[7] Wang, L.; Deng, R.; Li, J., Target-fueled DNA walker for highly selective miRNA detection. *Chem. Sci.* **2015,** *6* (12), 6777-6782.

[8] Wang, Q.; Yin, B.-C.; Ye, B.-C., A novel polydopamine-based chemiluminescence resonance energy transfer method for microRNA detection coupling duplex-specific nuclease-aided target recycling strategy. *Biosens. Bioelectron.* **2016,** *80*, 366-372.